Near-infrared free carrier absorption in heavily doped silicon

Simeon C. Baker-Finch, Keith R. McIntosh, Di Yan, Kean Chern Fong, and Teng C. Kho

Citation: Journal of Applied Physics **116**, 063106 (2014); doi: 10.1063/1.4893176
View online: http://dx.doi.org/10.1063/1.4893176
View Table of Contents: http://scitation.aip.org/content/aip/journal/jap/116/6?ver=pdfcov
Published by the AIP Publishing

Near-infrared free carrier absorption in heavily doped silicon

Simeon C. Baker-Finch,[1,2,a)] Keith R. McIntosh,[2] Di Yan,[1] Kean Chern Fong,[1] and Teng C. Kho[1]
[1]*School of Engineering, Australian National University, Canberra, ACT 0200, Australia*
[2]*PV Lighthouse, Coledale, NSW 2515, Australia*

(Received 10 May 2014; accepted 4 August 2014; published online 13 August 2014)

Free carrier absorption in heavily doped silicon can have a significant impact on devices operating in the infrared. In the near infrared, the free carrier absorption process can compete with band to band absorption processes, thereby reducing the number of available photons to optoelectronic devices such as solar cells. In this work, we fabricate 18 heavily doped regions by phosphorus and boron diffusion into planar polished silicon wafers; the simple sample structure facilitates accurate and precise measurement of the free carrier absorptance. We measure and model reflectance and transmittance dispersion to arrive at a parameterisation for the free carrier absorption coefficient that applies in the wavelength range between 1000 and 1500 nm, and the range of dopant densities between $\sim 10^{18}$ and $3 \times 10^{20}\,\mathrm{cm}^{-3}$. Our measurements indicate that previously published parameterisations underestimate the free carrier absorptance in phosphorus diffusions. On the other hand, published parameterisations are generally consistent with our measurements and model for boron diffusions. Our new model is the first to be assigned uncertainty and is well-suited to routine device analysis. © *2014 AIP Publishing LLC*. [http://dx.doi.org/10.1063/1.4893176]

I. INTRODUCTION

Free carrier absorption involves the transfer of photon energy to an electron or hole in the semiconductor conduction or valence band, respectively. Excited electrons transition to a state in the same or another conduction band. Holes make similar transitions in the valence bands. Naturally, free carrier absorption is stronger in semiconductors with high electron or hole concentrations, such as heavily doped[1] or highly injected silicon.[2] At near-bandgap photon energies, where band-to-band absorption is weak, free carrier absorption can contribute significantly to the total absorption in the semiconductor. In the case of silicon, the onset of this effect is in the near infrared (photon wavelengths above ~1000 nm).

Free carrier absorption is usually identified as a parasitic process—it has a negative impact on the performance of devices such as silicon solar cells,[3] thermophotovoltaic cells,[4] and infrared photodetectors.[5] On the other hand, when its relationship to free carrier density and wavelength is well-parameterised, free carrier absorption provides a means to characterize or monitor electron-hole plasmas (i.e., free carrier density)[2] and implanted or diffused silicon.[1,6]

Although the fundamental theory[7] and quantum-mechanical extensions (see, e.g., Refs. 8 and 9) are well-established, there exists a large discrepancy between the free carrier absorption predicted by numerous published parameterisations for heavily doped silicon in the infrared.[1,6,10–12] We examine, for example, the free carrier absorptance of the heavily phosphorus diffused front surface of a contemporary industrial silicon solar cell. We assume that the diffusion has 70 Ω/sq sheet resistance, that the phosphorus concentration at the surface is $2 \times 10^{20}\,\mathrm{cm}^{-3}$, and that the depth-dependence of the concentration follows a Gaussian function. In this exemplary case, the five parameterisations cited above predict absorption of between 0.2 and 1.0% of 1200 nm light traversing the diffusion at an angle normal to the surface. Moreover, as we demonstrate later, all published parameterisations underestimate the free carrier absorption measured experimentally in this study. Our contention is that the available parameterisations of free carrier absorption are either (i) not suited to routine assessment of silicon devices in the infrared or (ii) are derived from measurements of unknown precision.

In this work, we introduce the classical free carrier absorption theory and quantum variants in order to elucidate the genesis of the various aforementioned parameterisations of the free carrier absorption coefficients. We prepare large sets of boron- and phosphorus-diffused silicon wafers, and then apply spectrophotometry to determine the free carrier absorptance of near infrared radiation in these diffused regions. We derive a new parameterization for the free carrier absorption coefficient in silicon that is applicable to dopant densities between $\sim 10^{18}$ and $3 \times 10^{20}\,\mathrm{cm}^{-3}$ and wavelengths between 1 and 1.5 μm. We pay attention to measurement uncertainty, thereby elucidating the potential origin of apparently vast discrepancies between previously published parameterisations.

II. FCA THEORY

The phenomenon of free carrier absorption occurs when an electron (hole) in the conduction (valence) band of a semiconductor absorbs a photon, thus making a transition to a higher (lower) energy state within that band. Such a transition is assisted by an additional momentum-conserving process. That is, simultaneously as the photon is absorbed by the free carrier, a phonon must be emitted or absorbed, or the carrier must be scattered from an ionised impurity centre.[13,14]

a)e-mail address: simeon.bakerfinch@gmail.com

The classical theory of free carrier absorption is derived from Drude's simple model for the harmonic oscillation of unbound electrons in a fixed array of scattering nuclei (or the harmonic oscillation of the electric field of light interacting with an array of electrons).[15] Under the simplifying assumption of this model, namely that the binding energies of the nuclei approach zero, the oscillator damping term is inversely proportional to the mean time τ between collisions of the oscillating particles and the nuclei.[7,13,14,16,17] Note that τ is independent of the energy (and thereby the wavelength, λ) of the exciting photon. The resulting free carrier absorption coefficient α_{FCA} is[7,13]

$$\alpha_{FCA} = \frac{N\lambda^2 q^2}{4\pi^2 \varepsilon_0 m_c c^3 n \tau}, \tag{1}$$

where N is the concentration of free carriers, λ is the free-space wavelength, q is the fundamental charge, ε_0 is the vacuum permittivity, m_c is the conductivity effective mass of the free carrier, c is the speed of light, and n is the real component of the semiconductor refractive index.

Smith[7] describes a semi-classical extension to this model, whereby the right hand side of Eq. (1) is multiplied by an expectation value g. This allows one to account for the change in scattering mechanism with energy, and hence, the change in τ with λ. The value of g was derived by Schumann and Phillips[18] for the case of ionised impurity scattering following the Conwell–Weisskopf approximation (scattering events are independent);[19] the Schumann *et al.* analysis forms the theoretical basis of the parameterisation of Isenberg and Warta.[6] Experimental work found g to be twice as large for carrier–carrier interactions than carrier–impurity interactions.[2]

The Drude theory (and its semi-classical extension) provides a simple theoretical framework for free carrier absorption, but possesses several deficiencies.[20] It is derived under the condition that the semiconductor energy surface is spherically symmetric and non-degenerate;[16] the actual band structure (e.g., in Si) is more complex. Additionally, the Drude theory is accurate only when (i) the magnitude of the energy absorbed by free carriers is small compared with the mean carrier energy (implying $\lambda > \sim 180\,\mu$m in Si at 300 K assuming $\tau > 10^{-13}$ s)[20] and (ii) when the relaxation time τ is independent of energy.[21] Finally, and most importantly in the context of the present study, the Drude theory does not consider the role of the third particle (a scattering impurity or phonon) in the photon-free carrier interaction.[8,9]

In practice, and in a quantum analysis, the collision interval τ depends on the nature of the scattering mechanism and the photon energy.[8,13,14,22–26] This can result in a λ-dependence of α_{FCA} that varies between $\lambda^{1.5}$ and $\lambda^{3.5}$ (rather than the λ^2 predicted by Drude theory) in the limits of phonon or ionised impurity scattering, respectively.[27] Pankove,[13] Seeger,[8] and Ridley[14] provide extensive background discussion in this regard. In general, several scattering modes coexist, with the dominant mode depending on the impurity concentration and species. It is usually reasonable to expect the exponent r in the dependence λ^r to increase with doping.[13]

III. PARAMETERISATIONS OF FCA IN HEAVILY DOPED SILICON

Experimental measurements of free carrier absorption in crystalline and polycrystalline silicon have been conducted since the 1950s (see, e.g., Ref. 28), for a range of applications. Since then, various parameterisations of α_{FCA} have been presented; they are summarized in Table I.

The earliest of these parameterisations was performed by Schroder *et al.*[1] The structure of Schroder's parameterisation follows from the Drude theory (i.e., α_{FCA} is proportional to λ^2), with additional assumptions, namely: (i) conductivity effective mass is constant with dopant or carrier concentration; (ii) mobility is constant with dopant or carrier concentration. Although the former assumption is well-supported for

TABLE I. Summary of parameterisations of the free carrier absorption coefficient in heavily boron- and phosphorus-doped silicon. Included are the results of this work, calculated via the procedure described below. Parameters are adjusted from their original published values so that the unit of λ is cm in every case, and α_{FCA} has units cm^{-1}. The uncertainty in parameters derived in this work represents a 95% confidence interval.

References	Equation for α_{FCA}	Parameter	Parameter value		λ range (μm)	N range (cm^{-3})
			p-Si	n-Si		
1	$CN\lambda^{\gamma}$	C	2.7×10^{-10}	1.0×10^{-10}	>4	$<10^{19}$
		γ	2	2		
10	$CN\lambda^{\gamma}$	C	2.6×10^{-10}	2.7×10^{-6}	<2.5	$\sim 10^{18}$
		γ	2	3		
6	$CN\lambda^2(1 + A\{1 + \mathrm{erf}[m \log(N/N_0)]\})$	C	10.72×10^{-11}	4.45×10^{-11}	1.2[a]	10^{16}–10^{20}
		A	2.59	5.75		
		m	0.76	0.67		
		N_0	3.2	6.3		
11	$CN\lambda^{\gamma}$	C	1.04×10^{-8}	4.52×10^{-8}	1–2	$\sim 10^{17}$–10^{20}
		γ	2.4	2.6		
12[b]	$CN\lambda^{\gamma}$	C	3.2×10^{-6}	3.0×10^{-6}	1–1.2	$\sim 10^{17}$–10^{20}
		γ	3	3		
This work	$CN\lambda^{\gamma}$	C	$(1.80 \pm 0.83) \times 10^{-9}$	$(1.68 \pm 0.62) \times 10^{-6}$	1–1.5	$\sim 10^{18}$–5×10^{20}
		γ	2.18 ± 0.01	2.88 ± 0.08		

[a]Isenberg and Warta[6] provide parameterisations for $\lambda = 1.2$, 5 and 8 μm, as well as a generic equation for arbitrary λ.
[b]The authors provided the values of C and γ in a personal communication.

$N < 10^{20}\,\mathrm{cm}^{-3}$,[29–31] the latter is inconsistent with various mobility models (e.g., Ref. 32) unless the applicable range of dopant concentrations is heavily restricted.[43] Indeed, the parameterisation given by Schroder *et al.* is based on measurements of α_{FCA} at $N < 10^{19}\,\mathrm{cm}^{-3}$. Its validity is also limited to $\lambda > 4\,\mu\mathrm{m}$, so the parameterisation is of little utility near the bandgap of silicon ($1.0 < \lambda < 1.5\,\mu\mathrm{m}$), and in the assessment of heavily doped regions (for example, in solar cells, where N often exceeds $10^{19}\,\mathrm{cm}^{-3}$ and approaches $\sim 10^{21}\,\mathrm{cm}^{-3}$).[6,33]

Following on from the work of Schroder *et al.*, various authors[10–12] adopt the approach of defining two constants C and γ, with the free carrier absorption coefficient taking the following dependence on N and λ:

$$\alpha_{FCA} = CN\lambda^{\gamma}. \tag{2}$$

With this general formula, the parameterisation is freed from the Drude theory restriction of $\gamma = 2$. That freedom typically allows improved fits to experimental measurements of α_{FCA}, particularly in heavily doped n-type silicon.[26]

One such parameterisation was given by Green[10] for carrier concentrations near $10^{18}\,\mathrm{cm}^{-3}$ and $\lambda < 2500\,\mathrm{nm}$. Later, Isenberg and Warta[6] developed a parameterisation for α_{FCA} with a more sophisticated theoretical basis. Rather than taking inspiration from the simple Drude theory (Eq. (1)) or following the general form of Eq. (2), they base their analysis on the semi-classical model (see Sec. II). Included in the parameterisation is a function including three fit parameters. This function mimics the expectation value $g\,(N,\lambda)$. Although the semi-classical model can be used to calculate α_{FCA} at any (λ, N), Isenberg and Warta provide parameter values only at selected wavelengths (1.2, 5, and 8 μm), and base the parameterisation on samples with $10^{16} < N < 10^{19}\,\mathrm{cm}^{-3}$. This limits the value of the parameterisation in routine simulation, where α_{FCA} must be rapidly calculated for a range of λ. In diffused silicon solar cells, for example, the range $1.0 < \lambda < 1.3\,\mu\mathrm{m}$ and $N \sim 10^{20}\,\mathrm{cm}^{-3}$ is of most importance.

In order to address the deficiencies of the previous work, Rüdiger *et al.*[11] sought to assess silicon solar cell-relevant free carrier absorption behavior. They developed a parameterisation for free carrier absorption based on reflectance measurements, focusing on near-infrared wavelengths ($\sim$1–2 μm) and doped regions of the kind found in typical devices. In an attempt to increase the sensitivity of their measurements to weak absorption, Rüdiger *et al.* chose structures (featuring surface texture and dielectric coatings) that increase the path length of light in the silicon substrates and diffusions. However, their approach was likely prone to significant uncertainty due to a complex sample structure, which introduces experimental error and necessitates otherwise avoidable assumptions in the associated modelling. Readily identifiable sources of potential error are (i) rounding or imperfection in the front texture realized on experimental samples not accounted for in ray trace modelling; (ii) use of a complex, potentially unphysical model for rear internal reflection at a partially polished surface; (iii) inhomogeneous diffused dopant concentration on texture not accounted for in modelling; (iv) the assumption that dopant concentration profiles at a planar (presumably {100}-oriented) surface is a reasonable proxy for the profile in a near-{111}-oriented pyramid facet; (v) potential spatial variation or uncertainty in thickness or composition of dielectric films on experimental samples not accounted for in modelling; and (vi) systematic underestimate of reflectance and transmittance incurred when weakly absorbed light passing multiple times across a sample at an oblique angle can be eventually coupled out of the sample at some location outside the integrating sphere opening port. In the present work, we mitigate these errors by measuring mechanically polished planar samples without dielectric coating.

Most recently, Xu *et al.*[12] parameterised free carrier absorption through very good fits of measured and modelled reflectance from silicon solar cell structures. The approach they employed was similar to that of Rudiger *et al.*, so was prone to the aforementioned uncertainties. Confidence in their parameterisation is limited by the small number of samples analysed.

In the subsequent sections of this work, we address the shortcomings of published parameterisations with an experimental methodology that is insensitive to many of the aforementioned sources of uncertainty. We arrive at a parameterisation that we believe to be well-suited to the analysis of doped regions for silicon solar cells and other devices for which near infrared behaviour is important. Additionally, our parameterisation is presented alongside an assessment of experimental precision.

IV. EXPERIMENTAL PROCEDURE

A. Sample preparation

The magnitude of FCA on heavily doped silicon in the near infrared was evaluated via the measurement of reflectance from and transmittance through a series of silicon wafers. These wafers were of $\sim$5 Ω cm resistivity, either 400 or 530 μm thick, and mechanically polished on both front and rear surfaces. Heavily doped regions were created via the symmetrical diffusion of either phosphorus (from $POCl_3$ vapour source) or boron (from BBr_3 vapour source) at high temperature in a quartz tube furnace. The numerous resultant concentration profiles examined in this study are shown in Figure 1. The figure plots the concentration of *substitutional* phosphorus or boron, measured with the electrochemical capacitance voltage (ECV) technique.[44] As is demonstrated, diffusion conditions were modified so as to achieve a range of doping profiles, with varying depths, and peak concentration ranging from 8×10^{18} to $3 \times 10^{20}\,\mathrm{cm}^{-3}$ or 2×10^{18} to $2 \times 10^{20}\,\mathrm{cm}^{-3}$ for phosphorus or boron, respectively. After diffusion, dilute HF immersion was used to remove the grown layer of phosphosilicate or borosilicate glass, revealing bare silicon. For each diffused sample or set of diffused samples, an undiffused equivalent reference wafer (with near identical thickness) was retained.

B. Measurement of reflectance and transmittance

The hemispherical reflectance R_{meas} and transmittance T_{meas} of both reference and diffused wafers were measured with a Perkin Elmer Lambda 1050 spectrophotometer with integrating sphere. Each quantity was measured at an angle

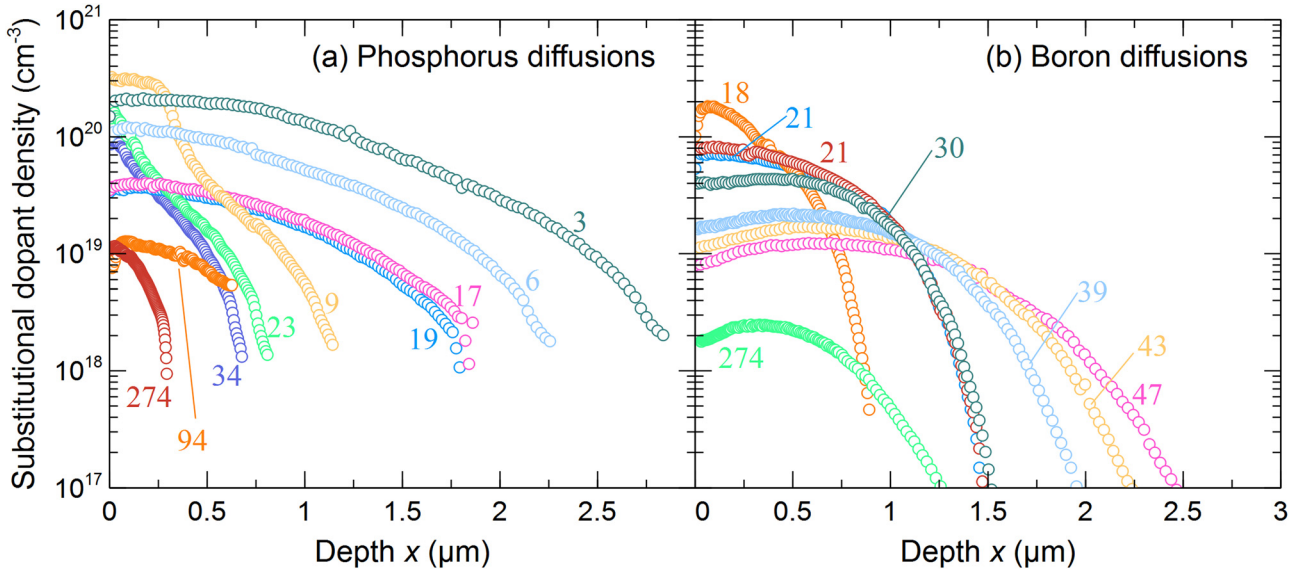

FIG. 1. Profiles of active dopant concentration of (a) phosphorus and (b) boron in the various diffused regions studied. The labels on the graph denote the sheet resistance (Ω/sq) of the diffused region.

of incidence of 8°, in wavelength intervals of 5 nm with 2 nm slit width in the range $800 < \lambda < 1500$ nm. The incident radiation is depolarized. The reflected or transmitted signal is detected by photomultiplier or InGaAs detector, and compared to a reference beam in order to correct for temporal fluctuations in the source beam. Intensity is calibrated to a white spectralon reflectance standard.

C. Extracting single-pass absorptance from reflectance and transmittance measurements

As is illustrated in Figure 2, R_{meas} and T_{meas} consist of the sum of light rays that have passed through the silicon wafer multiple times (or not at all, in the case of the first reflected ray). On each pass across the wafer, both band-to-band and free carrier absorption events take place, contributing to the reduction of intensity of the ray, so that $R_n < R_{n-1}$ and $T_n < T_{n-1}$. The strength of the carrier absorption events (i.e., the magnitude to which they reduce the intensity) depends on λ, and, in the case of free carrier absorption, on N or the profile of N across the wafer and in any surface diffusions. In order to isolate free carrier absorption and relate it in a meaningful way to N and λ, we extract the intensity reduction factor A (the "single-pass absorptance") from R_{meas} and T_{meas} following the procedure in Appendix 1.

To demonstrate the accuracy and limitations of our experimental technique, we extract $A(\lambda)$ for an undiffused silicon wafer of 400 μm thickness. The result is plotted as A_{ref} in Figure 3, where it is compared to A_{Green} calculated via the Beer-Lambert law for a wafer of this thickness and band-to-

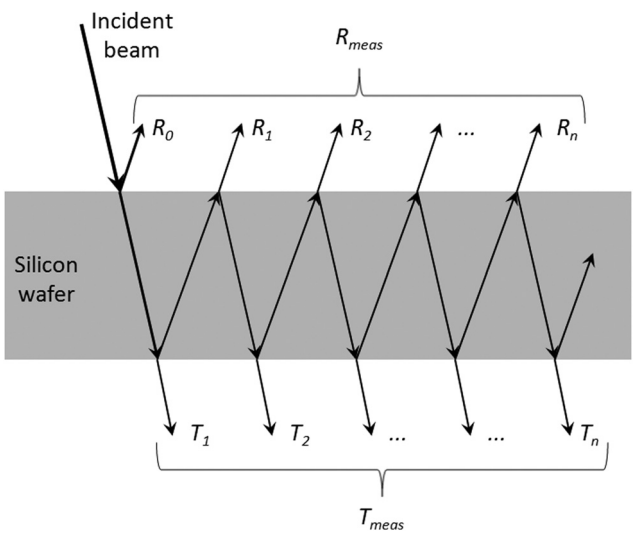

FIG. 2. Simple representation of the quantities (R_{meas} and T_{meas}) measured with spectrophotometry.

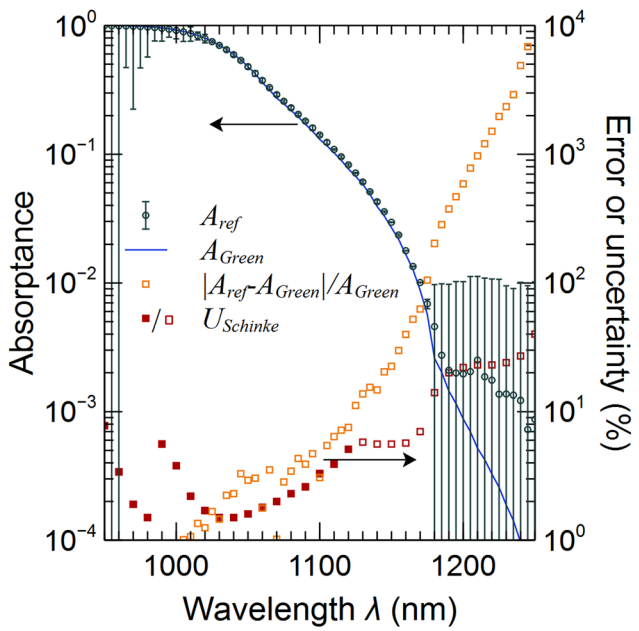

FIG. 3. Measured (A_{ref}) and modelled (A_{Green}) single pass absorptance across a 400 μm thick undiffused silicon wafer. The relative difference between measured and modelled quantities is plotted on the right-hand axis, where it is compared to an uncertainty analysis undertaken by Schinke *et al.*[37] Note that A_{ref} is imprecise at long wavelengths, where $A_{ref} < \sim 0.01$.

band absorption coefficients given by Green.[35,36,45] The figure additionally plots the relative deviation $(A_{ref}-A_{Green})/A_{Green}$ of our measurement from the calculated values. Predictably, the magnitude of the deviation increases as A_{ref} decreases; the precision in A_{ref} is governed by the experimental uncertainty in R_{meas} and T_{meas} is large when their sum is close to unity (note the large error bars on A_{ref} for $\lambda > 1180$ nm).

Notably, for $\lambda < 1120$ nm, the deviation follows the value $U_{Schinke}$ of the uncertainty in A_{ref} recently calculated by Schinke *et al.*[37] (refer to the symbols and right hand axis in Figure 3). At higher wavelengths, $U_{Schinke}$ refers to uncertainty in A_{ref} when measured by spectroscopic photoluminescence or solar cell spectral response, rather than spectrophotometry. The similarity of $(A_{ref}-A_{Green})/A_{Green}$ and $U_{Schinke}$ indicates that the deviation $A_{ref}-A_{Green}$ of our measurement from the theory could derive nearly entirely from uncertainty in A_{Green} (although it cannot be expected that experimental uncertainty in A_{ref} is zero).

More importantly, $(A_{ref}-A_{Green})/A_{Green}$ is less than 10% for $A_{ref} > 0.07$ and is below ~50% for $A_{ref} > 0.01$. This limitation on the sensitivity of our experimental approach and apparatus governs the range in which our measurement of free carrier absorption is reliable. As is shown later, this range is limited to $\lambda > 1000$ nm and $N > \sim 10^{18}$ cm^{-3}.

D. Extracting free carrier absorptance in a heavily doped region from single-pass absorptance

The total free carrier absorption $A_{FCA}(\lambda)$ in a heavily doped region is calculated via the following relationship between the single-pass absorptance $A(\lambda)$ for a symmetrically diffused sample and the reference single-pass absorptance $A_{ref}(\lambda)$

$$A_{FCA} = 1 - \sqrt{\frac{1-A}{1-A_{ref}}}. \tag{3}$$

Note that the determination of A_{FCA} via Eq. (3) does not require that the symmetrically diffused and reference samples have identical silicon-air interface reflectance. Therefore, our measurement is not affected through the Fresnel equations by any change in the real component of the refractive index of Si with dopant or carrier density.

Uncertainties in the measured A_{FCA} for a diffusion derive from uncertainties in A and A_{ref}, and, therefore, from the measured quantities R_{meas} and T_{meas}. We define the uncertainty δA_{FCA} in terms of δR_{meas} and δT_{meas} in accordance with the procedure described in Appendix 2. The physical sources of δR_{meas} and δT_{meas} are predominantly (i) the limited intensity resolution, nonlinearities, and calibration error in the detectors of the spectrophotometer and (ii) inhomogeneities (e.g., surface imperfections and thickness variation) across the sample, since R_{meas} and T_{meas} are acquired at slightly different locations on a sample. The limited resolution of the spectrophotometer has the largest impact on the certainty of our parameterisation, since as T_{meas} approaches zero or $T_{meas}+R_{meas}$ approaches unity to within that resolution, the uncertainty in that measured quantity approaches infinity. Note that, later in this paper, we deal separately with the uncertainty introduced by the concentration profile of dopants in the diffused regions (and their potential deviation from ECV measurement, variation across the sample surface, variation between front and rear surfaces and the like).

An exemplary data set is introduced in Figure 4. It relates to a boron-diffused wafer (diffusion has 30 Ω/sq sheet resistance). Directly measured quantities R_{meas} and T_{meas} are plotted alongside the calculated quantities introduced in the text, namely R, A, A_{ref}, and A_{FCA}.

V. SIMULATION PROCEDURE AND PARAMETERISATION

Having calculated A_{FCA} for numerous boron- and phosphorus-doped regions of silicon, we seek to determine an expression for α_{FCA} that predicts $A_{FCA}(N,\lambda)$. In the following sections, we (i) establish that good agreement with our experimental results can be achieved with a function of the form $\alpha_{FCA} = CN\lambda^{\gamma}$, where both C and γ are independent of N and λ; (ii) describe a technique for fitting a model of α_{FCA} to measurements of A_{FCA}; (iii) apply the technique to our large data set of measurements from boron- and phosphorus-diffused silicon; and finally (iv) present the resultant parameterization of α_{FCA}.

A. Choice of function for a parameterisation of the free carrier absorption coefficient

Previous parameterisations of α_{FCA}, summarised in Table I, take two distinct forms. The first, most common approach is to choose a function $f = CN\lambda^{\gamma}$ with two constants C and γ, both of which are independent of λ and N.[1,10,11] Usually, this limits the applicability of the parameterisation to a certain range of λ and N. As we discuss in Sec. II, the classical theory predicts α_{FCA} to exhibit linearity in N and a parabolic dependence on λ so that $a_{FCA} = CN\lambda^2$. However,

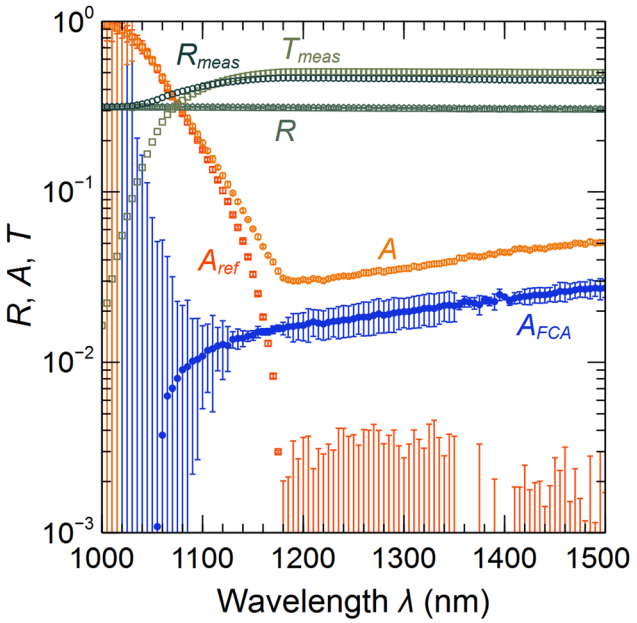

FIG. 4. An example of the measured quantities (R_{meas}, T_{meas}, and A_{ref}) and intermediate calculations (A) used to arrive at single pass free carrier absorption in a heavily doped region A_{FCA}. The data relate to the analysis of a boron diffused wafer.

quantum theory (and some experimental work) suggests that $\alpha_{FCA} \propto \lambda^{\gamma}$, where γ is not 2, and γ itself may be a function of N. The matter of the N-dependence of γ is investigated experimentally in this work, before the broader work of parameterising α_{FCA} is undertaken.

The second approach—applied by Isenberg and Warta[6]—is to parameterise α_{FCA} at a specific value of λ for a range of N. The function f may have the same form for various λ, but the parameters of f all vary with N and λ. Though it is well-suited to characterization performed at a single wavelength (e.g., measurement of free carrier density via IR laser transmission), this second approach becomes complex if the resultant parameterisation is to be applied in simulations in which a spectrum of wavelengths is incident on a device.

Given that we identify no clear advantage in the latter approach in initial fits to our measurements, we adopt the simpler first methodology. We do not, however, immediately assume that the parameters C and γ in $f = CN\lambda^{\gamma}$ are independent of N. Instead, we seek to confirm or deny such a dependence through experiment. In particular, we examined narrow heavily doped regions, across which N is nearly constant. To do so, we applied the measurement technique and analysis described in Sec. IV to a phosphorus-diffused silicon wafer from which very thin surface layers of thickness t were sequentially etched. By comparison of measurements before and after sequential surface layer removals, we isolate the free carrier absorption $A_{FCA(N)}$ occurring in the thin etched region. We then compute α_{FCA} from $A_{FCA(N)}$ via the inverse of the Beer-Lambert law

$$\alpha_{FCA}(N,\lambda) = \frac{-\ln\left(1 - A_{FCA(N)}\right)}{t}. \tag{4}$$

Next, by least squares fitting of α_{FCA} to the function $CN\lambda^{\gamma}$ for each thin layer, we find the relationship between γ and N. This relationship is plotted in Figure 5.

It is apparent that the classical $\gamma = 2$ dependence does not apply to our experimental measurements of α_{FCA} in phosphorus diffused silicon. Figure 5 indicates that the exponent γ is nearer to 3, thereby corroborating the parameterisations of Green,[10] Xu *et al.*,[12] and Rudiger *et al.*,[11] as well as experimental work (e.g., by Schmid[26]). Considerable scatter in our data is also apparent. The source of the scatter is the large uncertainty in $A_{FCA(N)}$. In this experiment, since the subsequently etched layers were very thin ($t \sim 10\,\text{nm}$), that uncertainty derives from the fact that we measured very small differential values of absorptance. A superior approach would involve the preparation and measurement of a set of relatively thick ($t > 1\,\mu\text{m}$) films of (e.g., epitaxially grown) doped silicon with controlled and constant N. Such an approach would also allow one to investigate the behavior of γ at $N < 10^{19}\,\text{cm}^{-3}$; our present approach breaks down in this regime, since free carrier absorptance in 10 nm of less heavily doped silicon is small and imprecisely detected.

For the purposes of our parameterization, we draw no clear conclusions from Fig. 5 with regard to a relationship between γ and N. We proceed by simplifying the problem—we assume that γ is independent of N in our samples (both for phosphorus and boron doped silicon). Confidence in the physical basis of our parameterization is limited for $N < 10^{19}\,\text{cm}^{-3}$, where we have no data for γ. However, we show later that choosing a constant γ does not preclude excellent fits of modelled α_{FCA} to experiment for lower N (10^{17}–10^{18} cm^{-3}). Furthermore, the linear dependence of α_{FCA} on N means that any such lack of confidence has little impact on device performance in most important cases (assuming that when α_{FCA} is small, it is less important).

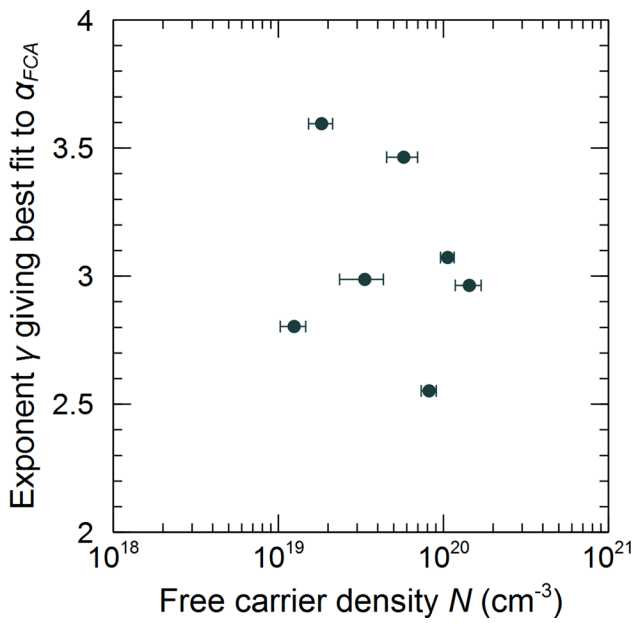

FIG. 5. Experimentally determined relationship between the λ-exponent γ and free carrier density in a phosphorus diffused region. No clear relationship is exposed, though the classical $\gamma = 2$ dependence is not apparent.

B. Modelling A_{FCA} and fitting to experiment

Having chosen the form $\alpha_{FCA} = CN\lambda^{\gamma}$, we seek to determine the optimal set (C, γ) of constant parameters to describe our experimental observations. This involves modelling the free carrier absorptance in heavily doped regions of varying dopant concentration, profile, and thickness, then fitting this model (via parameter variation) to measurements.

Each investigated heavily doped region is discretised into m elements of width Δx_1. Δx_m, with free carrier density assumed constant across each element and denoted N_1. N_m. We calculate the N_i by applying Altermatt *et al.*'s parameterisation for incomplete ionisation[38,39] to the ECV data.[34] We assume that since N does not vary across each element, neither does the local value of α_{FCA} for a given λ. The modelled free carrier absorption in a single pass across the heavily doped region is written as

$$A^{*}_{FCA}(\lambda) = 1 - \prod_{i=1}^{m} T_i, \tag{5}$$

where

$$T_i(\lambda) = \exp\left[-\alpha_{FCA}(\lambda, N_i) \cdot \Delta x_i\right]. \tag{6}$$

To determine the most appropriate values of C and p (in this exemplary for a single heavily doped region, but later,

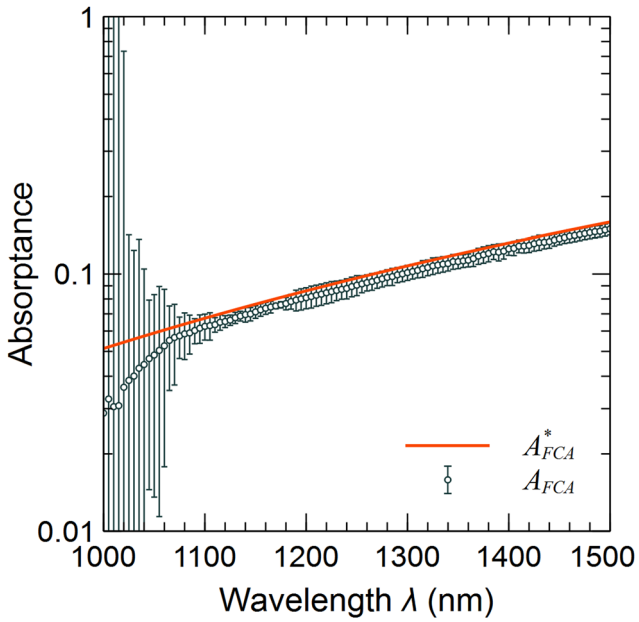

FIG. 6. Example of the fit to (measured) A_{FCA} by (modelled) A_{FCA}* when parameters C and γ are chosen to minimise the weighted-least-squares difference between the two. The example is for a phosphorus diffusion of 9 Ω/sq sheet resistance.

for the full set of regions), we minimise the uncertainty-weighted sum of square-differences between modelled and measured free carrier absorption. We consider the wavelengths λ_i at intervals of 5 nm between 1000 and 1500 nm (i.e., $\lambda_0 = 1050$ nm and $\lambda_{90} = 1500$ nm), so that the figure of merit e for the quality of the model fit to experiment is given by

$$e = \sum_{i=0}^{90} \frac{\left(A^*_{FCA} - A_{FCA}\right)^2}{\left(\Delta A_{FCA}/A_{FCA}\right)^2}. \tag{7}$$

The best fit for a single heavily diffused region occurs when γ and C are chosen such that e is minimised. For the phosphorus doped sample presented in Figure 6, we find a minimum $e = 8.3 \times 10^{-3}$ when $\gamma = 2.94$ and $C = 2.46 \times 10^{-6}$.

To extend the analysis from a single diffusion to the entire set of free carrier absorption measurements, we minimise a global figure of merit E. For a set of m measurements ($j = 1 \ldots m$), we define

$$E = \sum_{j=1}^{m} e_j, \tag{8}$$

where e_j is calculated with Eq. (7) for a given measurement.

C. Resultant parameterization for α_{FCA} and parameter uncertainty

The full set of measurements and their respective global best fits is presented in Figures 7(a) and 7(b) for phosphorus- and boron-doped regions, respectively. In terms of the free carrier absorption coefficient, we calculate

$$\alpha_{FCA,P} = 1.68 \times 10^{-6} N \lambda^{2.88} \tag{9}$$

and

$$\alpha_{FCA,B} = 1.82 \times 10^{-9} N \lambda^{2.18}. \tag{10}$$

We highlight, however, that the values of the parameters in Eqs. (9) ($C = 1.68 \times 10^{-6}$ and $\gamma = 2.88$) and (10) ($C = 1.82 \times 10^{-9}$ and $\gamma = 2.18$) are associated with additional uncertainty arising from our combined experimental and modelling approach. In particular, the use of experimentally determined N_i causes uncertainty in A_{FCA}* which propagate into C and γ. These uncertainties are quantified with a Monte Carlo simulation in Appendix 3. Through this Monte Carlo simulation, we additionally unveil a dependence of C on γ (refer to Eqs. (A5) and (A6)). Our complete model for

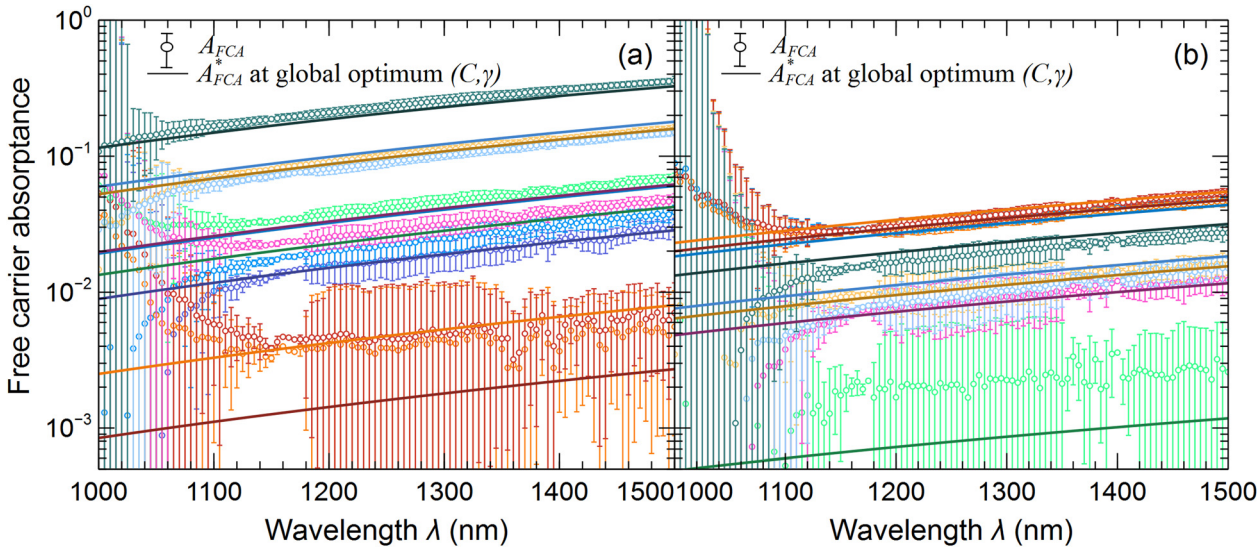

FIG. 7. Experimental measurements and global best fits to the free carrier absorptance in the near infrared for a range of (a) phosphorus and (b) boron doped regions. Markers (measurement) and lines (model) are plotted in similar colours. Marker colours correspond to the marker colours for the diffusion profiles in Figure 1.

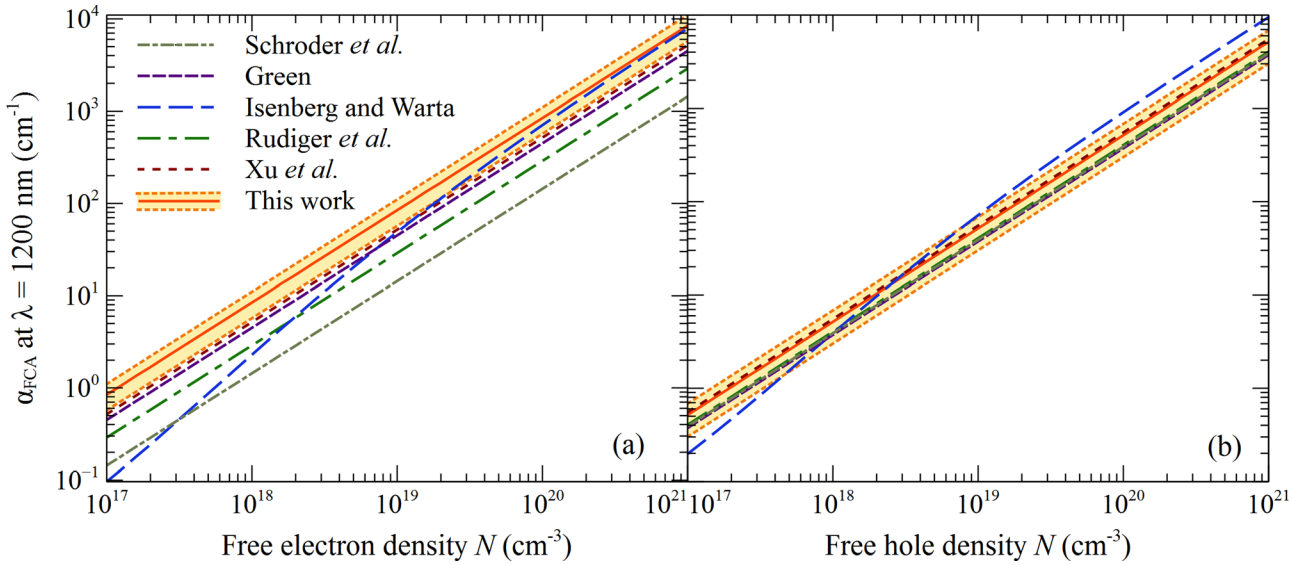

FIG. 8. Free carrier density dependence of the free carrier absorption coefficient at $\lambda = 1200$ nm in (a) phosphorus and (b) boron doped silicon. Published parameterisations are compared with the one developed in this work. The shaded yellow bands indicate the 95% confidence interval about our parameterisation, as described in the text and listed in Table I.

the free carrier absorption coefficient in heavily doped silicon in the near infrared is presented in Table I.

D. Comparison of parameterizations

Examining Table I, it is apparent that there exist rather large discrepancies between our parameterisations and those published in the past. In Figures 8 and 9, we compare α_{FCA} at either fixed wavelength ($\lambda = 1200$ nm) or fixed carrier density ($N = 10^{19}$ cm^{-3}). Focusing first on phosphorus doped material, it is apparent that our parameterisation indicates higher α_{FCA} than calculated by the alternatives. Our parameterisation and that of Isenberg and Warta[6] converges at $N > 10^{20}$ cm^{-3} for $\lambda = 1200$ nm. This is an interesting observation given that Isenberg and Warta's parameterisation was based on experimental data with $N < 10^{19}$ cm^{-3}. Potentially, their parameterisation is more accurate at $N < 10^{18}$ cm^{-3} than the one we present; our measurements of doped regions with varying concentration were inherently insensitive at low N, though given the sample set, this effect could not be captured in our uncertainty analysis. With regard to phosphorus doped silicon, the parameterisation of Isenberg and Warta appears to be a reasonable choice for free carrier absorption in the infrared. However, given that parameters are only supplied for $\lambda = 1200$ nm, our parameterisation may be a more practical choice for routine device simulation. We further conclude that the alternative published parameterisations would underestimate free carrier absorption in a heavily phosphorus doped region for $1000 < \lambda < 1500$ nm. We note however, that our parameterisation is, to our knowledge, the first to be provided with an associated calculation of uncertainty. Assuming identical uncertainty in the previously

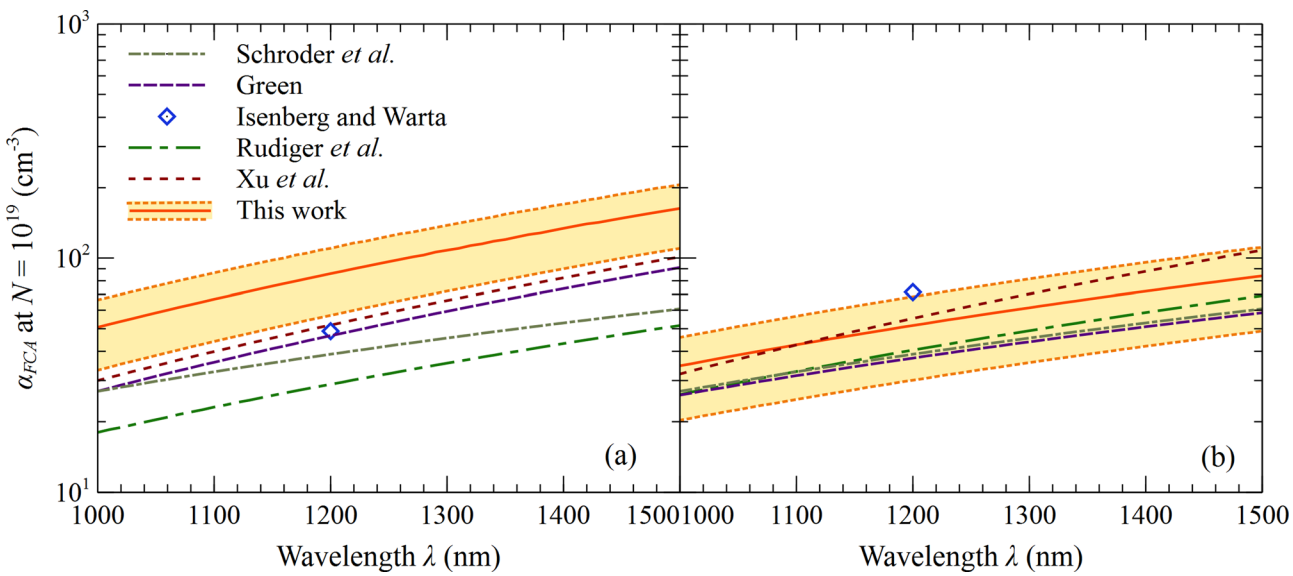

FIG. 9. Near infrared wavelength dependence of the free carrier absorption coefficient for an $N = 10^{19}$ cm^{-3} in (a) phosphorus and (b) boron doped silicon. The shaded yellow bands indicate the 95% confidence interval about our parameterisation, as described in the text and listed in Table I.

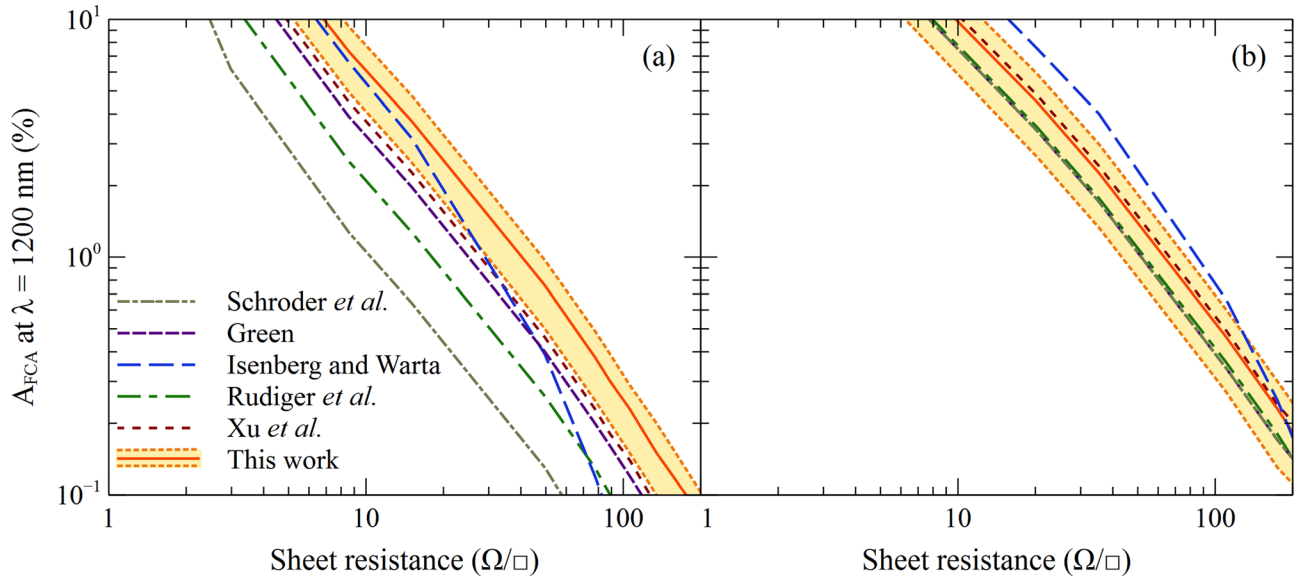

FIG. 10. Proportion of 1200 nm light absorbed by free carriers in a (a) phosphorus or (b) boron doped region with Gaussian concentration profile with varying surface concentration and depth factor 1 μm. Free carrier absorptance is calculated by applying a range of parameterisations for α_{FCA}.

published work would result in overlapping 95% confidence intervals for parameterisations including ours but excluding that of Schroder *et al.*[1]

On the other hand, for boron doped silicon, we find agreement between our parameterisation and several others for the full range of N and λ.[1,10–12] We additionally corroborate Isenberg and Warta's[6] analysis for $10^{18} < N < 10^{19}\,\mathrm{cm}^{-3}$. Again, our relative experimental insensitivity for $N < 10^{18}\,\mathrm{cm}^{-3}$ means that we cannot refute the Isenberg and Warta parameterisation in this range.

Note that our parameterisation is more consistent with others in the case of boron doping than phosphorus doping (though as we indicate earlier, many parameterisations are consistent to within calculated or assumed uncertainty). We are not yet able to attribute a physical mechanism or driving factor for this distinction between dopants. It is possible that precipitated phosphorus atoms have an optical impact that confounds our measurement or that of others. Precipitates could exist in very different concentrations in various sample sets depending on diffusion conditions. It is also possible that for the textured samples,[11,12] the conformance of the diffusion profile to the surface differs significantly for phosphorus and boron, with the effect resulting in a larger underestimate of α_{FCA} for phosphorus than boron.

E. Implications for practical doped regions

To attach practical relevance to the discrepancies between parameterisations, we use a simple, freely available online calculator[40] to simulate the free carrier absorptance in a range of heavily doped regions that might be achieved by diffusion or ion implantation. We consider light that passes normal to a silicon surface into which a Gaussian profile of dopants has been diffused. To vary sheet resistance, we vary surface concentration only, maintaining a constant (1 μm) standard deviation of the Gaussian.[46] We assume $\lambda = 1200$ nm, this wavelength being sufficiently near the silicon absorption band edge and sufficiently high to suffer from potentially measurable parasitic free carrier absorption. We thus predict a likely upper limit to the free carrier absorption that would be relevant to the operation of a device such as a solar cell or infrared photodetector.

The simulation results are plotted in Figure 10; as expected, the discrepancy between models, particularly when assessing phosphorus doped regions, is clear. Our parameterisation predicts slightly higher absorption in phosphorus doped regions. In an exemplary 78 Ω/sq region, our parameterisation gives $0.4 \pm 0.1\%$ absorptance; this is significantly higher than the absorptance calculated with all other models. For boron diffusions, our parameterisation predicts (to within its uncertainty) the absorptance calculated with almost the full suite of previously published parameterisations. The exception to the consistency of the data is that Isenberg and Warta predict up to 70% relative more free carrier absorption in very heavily boron doped regions (~10 Ω/sq).

VI. CONCLUSIONS

We determined experimentally, via reflection and transmission measurements, the free carrier absorptance of heavily phosphorus- and boron-doped silicon in the near infrared. Our choice of a simple sample structure (planar, diffused silicon wafers) contributes positively to the confidence with which we can extract free carrier absorptance from the measured quantities. We arrived at a parameterisation for the free carrier absorption coefficient α_{FCA} for each dopant type. Like various previous works,[1,10–12] we find an appropriate function for α_{FCA} with two constants, C and γ, which takes the form $\alpha_{FCA} = CN\lambda^{\gamma}$. Global best fits to 9 samples of a given dopant species were $(C, \gamma) = (1.68 \times 10^{-6}, 2.88)$ and $(C, \gamma) = (1.82 \times 10^{-9}, 2.18)$ for phosphorus and boron, respectively. We undertake an analysis of the uncertainty of the parameters; to our knowledge, this is the first such analysis. The majority of previously published parameterisations appears to underestimate the degree of free carrier absorption in heavily phosphorus doped silicon ($N > 10^{18}\,\mathrm{cm}^{-3}$) in the

infrared ($1000 < \lambda < 1500$ nm). On the other hand, when the dopant is boron, we find no significant difference between our parameterisation and those published in the past.

The parameterisation presented in this work is well-suited to routine analysis of devices in which near infrared free carrier absorption is an issue. The simulation of silicon solar cells, for example, will benefit from this parameterisation. Further improvement to the accuracy and precision of the free carrier absorption coefficient could be realised by applying our experimental methodology to epitaxial silicon, which can be grown to several microns of thickness with a constant and controllable dopant concentration. Particular focus could be applied to less heavily doped silicon ($N < 10^{18}\,\mathrm{cm}^{-3}$), to which the presented experiment was insensitive, and for which the precision of the current parameterisation is low.

ACKNOWLEDGMENTS

The authors wish to acknowledge Dr Fiacre Rougieux and Mr Hieu Nguyen from the Australian National University for productive discussion related to mobility and band-band absorptance, respectively.

APPENDIX: SUPPLEMENTARY CALCULATIONS

1. Extraction of single pass absorptance *A* from R_{meas} and T_{meas}

Extraction of A and R requires the solution of the simultaneous equations for measured R_{meas} and T_{meas}. These equations involve infinite sums of A and R (see Ref. 41 for an explanation). The resultant definitions of A and R are

$$A = \frac{RA_{meas} - A_{meas}}{RA_{meas} + R - 1}, \tag{A1}$$

where

$$A_{meas} = 1 - R_{meas} - T_{meas} \tag{A2}$$

and

$$R = \frac{-\left(1 + T_{meas}^2 + 2R_{meas} - R_{meas}^2\right) + \sqrt{\left(1 + T_{meas}^2 + 2R_{meas} - R_{meas}^2\right)^2 + 4(R_{meas} - 2)R_{meas}}}{2(R_{meas} - 2)}. \tag{A3}$$

2. Propagation of experimental uncertainty; from δR_{meas} and δT_{meas} to δA_{FCA}.

Uncertainties in the two measured quantities R_{meas} and T_{meas} propagate through to A_{FCA}. We measure random experimental error δR_{meas} and δT_{meas} by measuring reference silicon wafers 5 times, and define the uncertainty by a 95% confidence interval about the mean in the measured parameter at each λ. This uncertainty reflects the intensity resolution of the spectrophotometer, variation (e.g., in thickness, surface condition, or dopant concentration) across a sample, and drift in the source and sensing electronics of the spectrophotometer. Refer to Figure 3, where we showed that we were able to precisely measure the band to band absorption coefficient; this confirmed that our measurements do not possess additional systematic errors for which we must account.

Propagation of uncertainties from the measured quantities through to A is calculated by assuming normal distributions of uncertainty. Note that, per Eq. (3), A_{FCA} depends on A_{meas} for both the reference (A_{ref}) and diffused sample (A). The resultant uncertainty δA_{FCA} is given by

$$\delta A_{FCA} = \left(\left(\frac{1 - A}{1 - A_{ref}}\right)^{1/2} + 1/2\left(\frac{\delta A}{1 - A} + \frac{\delta A_{ref}}{1 - A_{ref}}\right)\right), \tag{A4}$$

where both δA and δA_{ref} are uncertainties propagated from the measured quantities through Eqs. (A1)–(A3).

3. Uncertainty in parameters *C* and γ of α_{FCA}

The modelled quantity A_{FCA}* depends on N_i (i.e., the profile of dopant concentration through which the light passes in our spectrophotometric analysis). The model is therefore uncertain, with its uncertainty linked to uncertainty δN_i in each N_i. Key potential sources for δN_i are (i) non-uniform dopant profiles across the sample (e.g., the location probed with spectrophotometry has a different concentration of dopants than the location probed with ECV) and (ii) uncertainties deriving from the ECV measurement. By measuring the sheet resistance of the heavily doped region with a four point probe at five locations across the sample, we determine that the former source contributes a$\sim$5% standard deviation.[47] An additional uncertainty of $\sim$5% derives from ECV measurement and is primarily related to the imprecise definition of electrode area (e.g., due to bubbles in the electrolyte or imperfection in the ring-seal) and, to a lesser degree, a parasitic contribution of the etched walls to the depletion capacitance.[42] Note that both key contributions to δN_i are dominated by uncertainty that scales N for all i; we therefore assume that for a given experimental sample $\delta N_i \equiv \delta N$ for all i. Note further that δN for each sample is independent (the nature of the key sources of uncertainty are such that N_i may be overestimated for one sample, and underestimated for the next).

To account for the impact of δN_i on γ and C, we performed a Monte-Carlo analysis. We assumed that N_i can vary from its measured value with a normal distribution having a standard deviation of 10% (i.e., $\delta N/N_i$ has normal

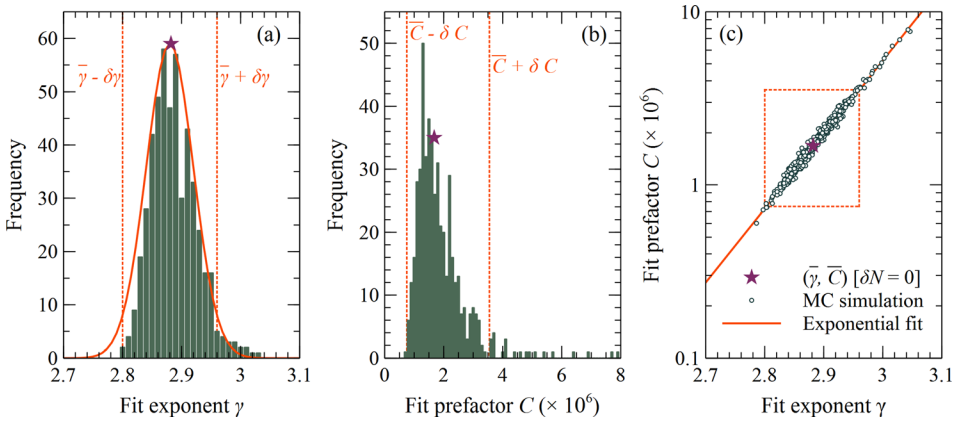

FIG. 11. Monte Carlo simulation results illustrating the impact of uncertainty in N on the fit parameters γ and C. In (a), the distribution of γ is compared with a normal distribution about the mean, which coincides with the value of γ when $\delta N = 0$. Dotted orange lines represent a 95% confidence interval around the value of that mean. In (b), the distribution of C is plotted, and displays a skewed distribution. The skew relates to the exponential relationship between γ and C, as is illustrated in (c).

distribution with zero mean and 0.1 standard deviation). In a single Monte Carlo run, each experimental sample was assigned a randomly selected value of $\delta N/N_i$ from the distribution, and a new "effective" N_i was determined. Next, the parameters γ and C were varied until E was minimised in accordance with the procedure described in Sec. V B; optimal values of γ and C were recorded. This process was repeated until 500 Monte-Carlo runs were performed.

Taking our set of phosphorus diffused samples as an example, we plot a frequency histogram γ in Figure 11(a). Note that the centre of the normal distribution value is equal to the value of γ presented in Eq. (9) (where zero uncertainty in N_i was assumed). We found, for phosphorus doped silicon, $\gamma = 2.88 \pm 0.08$ to be a 95% confidence interval. Performing the Monte Carlo simulations revealed that the prefactor parameter C is exponentially dependent on γ, per Figure 11(b). The distribution of C values is therefore not normal. Note that we account for the uncertainty in the parameters of this exponential fit, arriving at

$$C = (8.1 \pm 3.0) \times 10^{-19} \exp\left[(9.8 \pm 0.1)\gamma\right]. \quad \text{(A5)}$$

We follow the same procedure for boron doped silicon, to find

$$C = (1.3 \pm 0.6) \times 10^{-17} \exp\left[(8.6 \pm 0.2)\gamma\right]. \quad \text{(A6)}$$

In summary, accounting for uncertainties in γ and in its exponential relationship with C, we arrive at a 95% confidence interval for the FCA coefficient for phosphorus doped silicon

$$1.05 \times 10^{-6} N\lambda^{2.80} < \alpha_{FCA} < 2.30 \times 10^{-6} N\lambda^{2.96}; \quad \text{(A7)}$$

and for boron doped silicon

$$0.97 \times 10^{-9} N\lambda^{2.17} < \alpha_{FCA} < 2.64 \times 10^{-9} N\lambda^{2.19}. \quad \text{(A8)}$$

In Eqs. (A7) and (A8), N has units cm^{-3}, λ has units cm, and α_{FCA} has units cm^{-1}.

[1]D. K. Schroder, R. N. Thomas, and J. C. Swartz, "Free carrier absorption in silicon," IEEE J. Solid State Circuits **SC-13**(1), 180–187 (1978).
[2]C. M. Horwitz and R. M. Swanson, "The optical (free-carrier) absorption of a hole-electron plasma in silicon," Solid-State Electron. **23**, 1191–1194 (1980).
[3]T. Tiedje, E. Yablonovitch, G. D. Cody, and B. G. Brooks, "Limiting efficiency of silicon solar cells," IEEE Trans. Electron Devices **31**(5), 711–716 (1984).
[4]M. B. Clevenger, C. S. Murray, and D. R. Riley, "Spectral utilization in thermophotovoltaic devices," Mater. Res. Soc. Proc. **485**, 291–296 (1997).
[5]M. Casalino, G. Coppola, M. Iodice, I. Rendina, and L. Sirleto, "Near-infrared sub-bandgap all-silicon photodetectors: state of the art and perspectives," Sensors **10**, 10571–10600 (2010).
[6]J. Isenberg and W. Warta, "Free carrier absorption in heavily doped silicon layers," Appl. Phys. Lett. **84**(13), 2265–2267 (2004).
[7]R. A. Smith, *Semiconductors*, 2nd ed. (Cambridge University Press, Cambridge, UK, 1959), pp. 216–219.
[8]K. Seeger, *Semiconductor Physics: An Introduction*, 2nd ed. (Springer-Verlag, *Berlin*, 1982), pp. 343–345.
[9]H. C. Huang, S. Yee, and M. Soma, "Quantum calculations of the change of refractive index due to free carriers in silicon with nonparabolic band structure," J. Appl. Phys. **67**(4), 2033–2039 (1990).
[10]M. A. Green, *Silicon Solar Cells: Advanced Principles and Practice* (University of New South Wales, Sydney, Australia, 1995), p. 48.
[11]M. Rudiger, J. Greulich, A. Richter, and M. Hermle, "Parameterization of free carrier absorption in highly doped silicon for solar cells," IEEE Trans. Electron Devices **60**(7), 2156–2163 (2013).
[12]G. Xu, Y. Yang, K. Zhang, W. Liu, S. Fu, Z. Feng, and P. Verlinden, "An improved optical simulation method for crystalline silicon solar cells," in *Proceedings of the 39th IEEE Photovoltaic Specialists Conference* (2013), pp. 2677–2680.
[13]J. I. Pankove, *Optical Processes in Semiconductors* (Dover Publications, New York, 1971), p. 74.
[14]B. K. Ridley, *Quantum Processes in Semiconductors* (Clarendon Press, Oxford, 1982), pp. 217–223.
[15]P. Drude, Ann. Phys. **306**, 566 (1900).
[16]A. H. Kahn, "Theory of the infrared absorption of carriers in germanium and silicon," Phys. Rev. **97**(6), 1647–1652 (1955).
[17]C. Drake, S. Deshpande, and S. Seal, "Determination of free carrier density and space charge layer variation in nanocrystalline In^{3+} doped tin oxides using Fourier transform infrared spectroscopy," Appl. Phys. Lett. **89**, 143116 (2006).
[18]P. A. Schumann and R. P. Phillips, "Comparison of classical approximations to free carrier absorption in semiconductors," Solid-State Electron. **10**, 943–948 (1967).
[19]E. M. Conwell and V. F. Weisskopf, "Theory of impurity scattering in semiconductors," Phys. Rev. **77**(3), 388–390 (1950).
[20]A. F. Gibson, "Infra-red and microwave modulation using free carriers in semiconductors," J. Sci. Instrum. **35**, 273–278 (1958).
[21]M. van Exeter and D. Grischkowsky, "Carrier dynamics of electrons and holes in moderately doped silicon," Phys. Rev. B **41**(17), 12140–12149 (1990).
[22]S. Hava and M. Auslender, "Theoretical dependence of infrared absorption in bulk-doped silicon on carrier concentration," Appl. Opt. **32**(7), 1122–1125 (1993).
[23]E. Barta and G. Lux, "Calculated and measured infrared reflectivity of diffused/implanted p-type silicon layers," J. Phys. D: Appl. Phys. **16**, 1543–1553 (1983).
[24]G. E. Jellison, F. A. Modine, C. W. White, R. F. Wood, and R. T. Young, "Optical properties of heavily doped silicon between 1.5 and 4.1 eV," Phys. Rev. Lett. **46**(21), 1414–1417 (1981).

[25]A. Slaoui and P. Siffert, "Determination of the electron effective mass and relaxation time in heavily doped silicon," Phys. Status Solidi A **89**, 617–622 (1985).
[26]P. E. Schmid, "Optical absorption in heavily doped silicon," Phys. Rev. B **23**(10), 5531–5536 (1981).
[27]H. Y. Fan, W. Spitzer, and R. J. Collins, "Infrared absorption in n-type germanium," Phys. Rev. **101**(2), 566–572 (1956).
[28]W. Spitzer and H. Y. Fan, "Infrared absorption in n-type silicon," Phys. Rev. **108**(2), 268–271 (1957).
[29]W. G. Spitzer, F. A. Trumbore, and R. A. Logan, "Properties of heavily doped n-type germanium," J. Appl. Phys. **32**(10), 1822–1830 (1961).
[30]G. E. Jellison, S. P. Withrow, J. W. McCamy, J. D. Budai, D. Lubben, and M. J. Godbole, "Optical functions of ion-implanted, laser-annealed heavily doped silicon," Phys. Rev. B **52**(20), 14607–14614 (1995).
[31]D. M. Riffe, "Temperature dependence of silicon carrier effective masses with application to femtosecond reflectivity measurements," J. Opt. Soc. Am. B **19**(5), 1092–1100 (2002).
[32]D. B. M. Klaassen, "A unified mobility model for device simulation - I. Model equations and concentration dependence," Solid-State Electron. **35**(7), 953–959 (1992).
[33]P. Hanselaer, S. Forment, L. Frisson, and J. Poortmans. "Near IR absorption in diffused layers of Si p-n junction solar cells," in *Proceedings of the 16th European Photovoltaic Solar Energy Conference* (2000), pp. 1348–1351.
[34]F. Huster and G. Schubert, "ECV doping measurements of aluminium alloyed back surface fields," in *Proceedings of the 20th European Photovoltaic Solar Energy Conference and Exhibition* (2005), pp. 1462–1466.
[35]M. A. Green, "Self-consistent optical parameters of intrinsic silicon at 300K including temperature coefficients," Sol. Energy Mater. Sol. Cells **92**, 1305–1310 (2008).
[36]H. T. Nguyen, F. E. Rougieux, B. Mitchell, and D. Macdonald, "Temperature dependence of the band-band absorption coefficienc in crystalline silicon from photoluminescence," J. Appl. Phys. **115**(4), 043710 (2014).
[37]C. Schinke, K. Bothe, P. C. Peest, J. Schmidt, and R. Brendel, "Uncertainty of the coefficient of band-to-band absorption of crystalline silicon at near-infrared wavelengths," Appl. Phys. Lett. **104**, 081915 (2014).
[38]P. P. Altermatt, A. Schenk, and G. Heiser, "A simulation model for the density of states and for incomplete ionization in crystalline silicon I. Establishing the model in Si:P," J. Appl. Phys. **100**, 113714 (2006).
[39]P. P. Altermatt, A. Schenk, B. Schmithusen, and G. Heiser, "A simulation model for the density of states and for incomplete ionization in crystalline silicon II. Investigation of Si:As and Si:B and usage in device simulation," J. Appl. Phys. **100**, 113715 (2006).
[40]*Free Carrier Absorption Calculator*, see www.pvlighthouse.com.au, accessed 28 April, 2014.
[41]E. Nichelatti, "Complex refractive index of a slab from reflectance and transmittance: analytical solution," J. Opt. A: Pure Appl. Opt. **4**, 400–403 (2002).
[42]R. Bock, P. P. Altermatt, and J. Schmidt, "Accurate extraction of doping profiles from electrochemical capacitance voltage measurements," in *Proceedings of the 23rd European Photovoltaic Solar Energy Conference* (2008), pp. 1510–1513.
[43]Variation in mobility with dopant concentration from 10^{17} to $10^{20}\,\mathrm{cm}^{-3}$ per Klaassen's model would alone drive a factor of 6 or 10 increase in α_{FCA} in heavily boron- and phosphorus-doped regions, respectively.[32]
[44]ECV measures the substitutional (or "active") dopant concentration, as opposed to the atomic concentration (as would be measured by, for example, secondary ion mass spectrometry). Additionally, note that the substitutional concentration can be larger than the ionised dopant concentration at a given temperature and dopant concentration. ECV measurements drive the surface into depletion to measure dopant concentration; under depletion conditions, the Fermi level moves towards mid-gap, so all dopant states are occupied, forcing complete ionisation.[34]
[45]Very similar curves for A_{ref} could be drawn by applying the more recent absorption coefficient data of Nguyen *et al.*[36] or Schinke *et al.*[37]
[46]Note that the free carrier absorptance is, to first order, dependent on the sheet resistance. For this demonstration, we might equally have chosen a 100 nm depth factor (and higher surface concentrations) to calculate similar, though not identical results.
[47]Assuming that N_i is proportional to sheet resistance. This is a reasonable assumption since for our profiles of interest, N_i do not lie in regions of rapidly varying mobility.